Observation of Subdiffusive Dynamic Scaling in a Driven and Disordered Bose Gas

Gevorg Martirosyan, Christopher J. Ho, Jiří Etrych, Yansheng Zhang, Alec Cao,*
Zoran Hadzibabic, and Christoph Eigen†
Cavendish Laboratory, University of Cambridge, J. J. Thomson Avenue, Cambridge CB3 0HE, United Kingdom

(Received 4 May 2023; accepted 5 January 2024; published 11 March 2024)

We explore the dynamics of a tuneable box-trapped Bose gas under strong periodic forcing in the presence of weak disorder. In absence of interparticle interactions, the interplay of the drive and disorder results in an isotropic nonthermal momentum distribution that shows subdiffusive dynamic scaling, with sublinear energy growth and the universal scaling function captured well by a compressed exponential. We explain that this subdiffusion in momentum space can naturally be understood as a random walk in energy space. We also experimentally show that for increasing interaction strength, the gas behavior smoothly crosses over to wave turbulence characterized by a power-law momentum distribution, which opens new possibilities for systematic studies of the interplay of disorder and interactions in driven quantum systems.

DOI: 10.1103/PhysRevLett.132.113401

Complex microscopic behavior of both classical and quantum systems can often be characterized by universal statistical properties. While such descriptions are more commonly associated with thermodynamic equilibrium, far-from-equilibrium systems, from kicked rotors and chaotic billiards [1–4] to turbulent fluids [5–7], can also display emergent universal behavior. A fascinating manifestation of this is dynamic scaling, which is akin to the scale invariance of equilibrium systems close to a phase transition, but generalized to scaling in both space and time. Such behavior is known from surface growth [8,9] and both normal and anomalous diffusion [10,11]. Recently, dynamic scaling was observed in a variety of quantum systems and in different scenarios [12–24], including the relaxation of atomic gases [13,14,16,18,21–24] and polariton systems [20], and the buildup of wave turbulence in a driven interacting Bose gas [17]. These experiments provide mounting evidence for the hypothesis that such scaling is generic to far-from-equilibrium quantum systems [25].

Usually interactions are at the heart of the emergent dynamics, but naturally present disorder can also play a crucial role. The study of disorder is a vast field, with highlights including localization and quantum-Hall phenomena in 2D electron gases and quantum wires [26–30], coherent backscattering of acoustic and electromagnetic waves [31,32], and Anderson localization of cold atoms [33,34]. Moreover, the interplay of disorder and interactions can result in new phenomena such as many-body localization in lattice systems [35–37] and time crystals [38–41].

In this Letter, we explore the dynamics of a 3D box-trapped Bose gas strongly driven in presence of weak

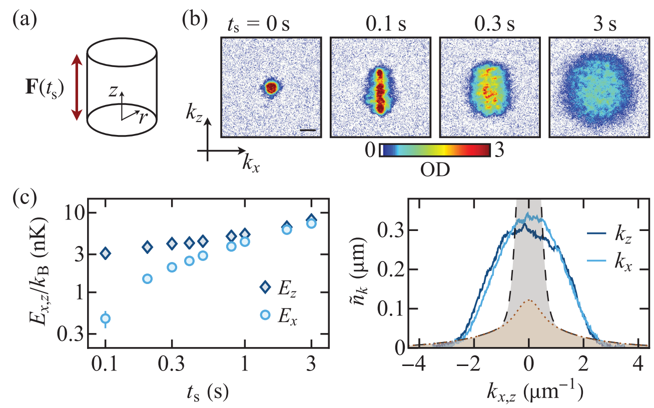

FIG. 1. Noninteracting box-trapped Bose gas driven far from equilibrium. (a) Box geometry and driving force, $\mathbf{F} = (U_s/L)\cos(\omega_s t_s)\hat{\mathbf{z}}$, where $L \approx 50$ μm is the box length. (b) Time-of-flight images, giving 2D momentum distributions $n_k(k_x, k_z)$, for $N = 3.3 \times 10^5$ atoms in a box of depth $U_D/k_B = 90$ nK, driven at $\omega_s/(2\pi) = 10$ Hz with $U_s/k_B = 10.5$ nK. The scale bar shows 1 μm^{-1} and the optical density (OD) saturates at 3. (c) Energies, $E_{x,z}$, and 1D momentum distributions, $\tilde{n}_k(k_{x,z})$, obtained by integrating 2D distributions over k_z or k_x; note that $E_x \approx E_z$ at $t_s = 0$. The axial E_z initially (in < 0.1 s) rises far above E_x, but at long t_s the two energies are almost equal and grow in unison. The long-time momentum distribution is essentially isotropic [$\tilde{n}_k(k_x) \approx \tilde{n}_k(k_z)$], but highly nonthermal. We show $\tilde{n}_k(k_{x,z})$ for $t_s = 3$ s, together with the calculated equilibrium distribution for the same energy per particle, $E/k_B \approx 23$ nK (shaded curve); the experimental distributions show no condensate peak, even though the condensation temperature is 180 nK and the equilibrium distribution has 66% condensed fraction (gray) [52].

disorder. In absence of interatomic interactions the gas shows subdiffusive dynamic scaling: its energy grows sublinearly with the drive time t_s, approximately as $t_s^{0.5}$, and its momentum distribution at different t_s is described by a scaling function that is captured well by an isotropic compressed exponential. This behavior is in stark contrast to that expected for a disorder-free noninteracting gas in our cylindrical geometry with forcing along the box axis [see Fig. 1(a)]; in that case the system is effectively 1D and one expects chaotic dynamics with bounded energy growth [42–44]. Our observations can be explained in terms of a random walk in energy space (see Ref. [45] for our detailed theoretical study) and give credence to the proposals that such random walks are a generic feature of thermally isolated driven systems [46–48]. We also experimentally show, by tuning the interaction strength, that the energy-space random walk observed in the noninteracting limit is continuously connected to wave turbulence characterized by a power-law scaling function [17,49–51]. This points to interesting future studies in the regime where the drive, the disorder, and the interactions all play a significant role.

We start with a quasipure ^{39}K Bose-Einstein condensate (BEC) in the lowest hyperfine state, trapped in a cylindrical optical box [54–56]. The condensate is prepared at a scattering length $a = 200\ a_0$ (where a_0 is the Bohr radius), and we slowly (in 5 s) tune a to zero by tuning the bias magnetic field to 350.4(1) G [57,58]. For a noninteracting BEC in our box of length $L \approx 50\ \mu$m and radius $R \approx 15\ \mu$m, the frequency of the lowest-lying axial excitation is (ignoring disorder) $\omega_z = 3\pi^2\hbar/(2mL^2) \approx 2\pi \times 1.5$ Hz, where m is the atom mass, while our variable trap depth U_D is always larger than $2\pi\hbar \times 400$ Hz. Weak optical disorder, proportional to the trapping laser power and hence U_D, is always present in our holographically created trap [54,59,60], but is typically irrelevant in interacting-gas experiments [61]. We inject energy into the system along the box axis $\mathbf{z}$, using a spatially uniform time-varying force [49] of magnitude $F(t_s) = (U_s/L)\cos(\omega_s t_s)$, with $\omega_s > \omega_z$ and $\hbar\omega_z \ll U_s \ll U_D$ (see also [42]). After driving the gas for a variable time t_s, we probe its momentum distribution using absorption imaging after 50 ms of time-of-flight expansion [53]; this gives line-of-sight integrated 2D distributions $n_k(\mathbf{k})$, which we normalize such that $\int n_k(\mathbf{k})d\mathbf{k} = 1$.

In Figs. 1(b) and 1(c) we illustrate our qualitative observations; here $E_{x,z} = \int \hbar^2 k_{x,z}^2/(2m) n_k(k_x, k_z) d\mathbf{k}$ and 1D momentum distributions, $\tilde{n}_k(k_{x,z})$, are obtained by integrating $n_k(\mathbf{k})$ over k_z or k_x. Initially the dynamics is essentially 1D, with the drive rapidly (in < 0.1 s) increasing only E_z. This is what is expected in absence of disorder, in which case the growth of E_z would be bounded [42]. However, at long times $E_x \approx E_z$ and the energy keeps growing. The long-time momentum distributions along k_x and k_z are nearly identical, but far from thermal; they show no BEC peak even though the energy per particle is far below the equilibrium condensation value.

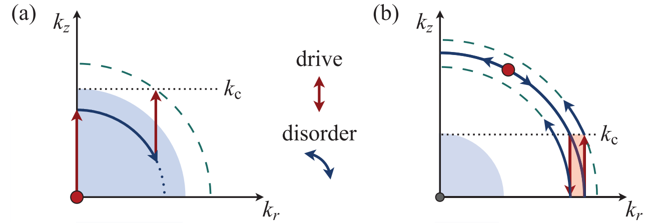

FIG. 2. Semiclassical picture of a driven and disordered noninteracting Bose gas. (a) The drive mixes only states with k_z values up to some k_c [42], so in absence of disorder the radial momentum k_r (in the k_x-k_y plane) remains zero, and the growth of a particle's energy is bounded by $E_c = \hbar^2 k_c^2/(2m)$. However, disorder-induced elastic scattering distributes energy into the radial modes, and allows the drive to populate states above E_c (outside the blue shaded area). (b) This picture implies subdiffusive long-time dynamics, with a sublinear energy growth. Here we consider a particle (red dot) that already has an energy above E_c, and $k_z > k_c$, so it does not interact with the drive. If elastic scattering (solid circle) reduces its k_z to below k_c, the particle temporarily interacts with the drive, until another scattering event increases its k_z above k_c. The interaction with the drive can either increase or decrease the particle's energy, as exemplified by the red arrows. The alternation of scattering and driving events thus results in an energy-space random walk, with a characteristic step size E_c.

In Fig. 2(a) we outline a semiclassical picture of how the interplay of the drive and disorder can lead to isotropic dynamics with unbounded energy growth. The drive mixes only axial modes, with k_z up to some k_c [42]. The disorder-induced elastic scattering transfers energy into the radial modes and allows the drive to increase a particle's energy above $E_c = \hbar^2 k_c^2/(2m)$. Alternating scattering and driving events then lead to an unbounded energy growth.

In Fig. 2(b) we explain why at long times this growth is sublinear, corresponding to subdiffusion in momentum space. Once the average energy per particle, E, is significantly larger than E_c, most particles have $k_z > k_c$ and do not interact with the drive. When a particle is occasionally scattered in and out of the $k_z < k_c$ space, its temporary interaction with the drive can either increase or decrease its energy (red arrows). This results in an energy-space random walk with a characteristic step size E_c [45]:

$$\frac{d}{dt_s}(E^2) \propto r(E) E_c^2. \qquad (1)$$

The rate r is energy-dependent, because at any time only a fraction of particles $\propto \hbar k_c/\sqrt{2mE}$ interacts with the drive, and because the density of states for elastic scattering is $\propto \sqrt{E}$. As shown in Ref. [45], this model predicts $E \propto t_s^{\eta}$, with $2/5 \leq \eta \leq 1/2$ depending on the ratio of the elastic scattering rate and the rate at which the drive mixes k_z states.

To isolate and quantify the disorder-induced scattering in our system, we prepare an anisotropic n_k using a short t_s,

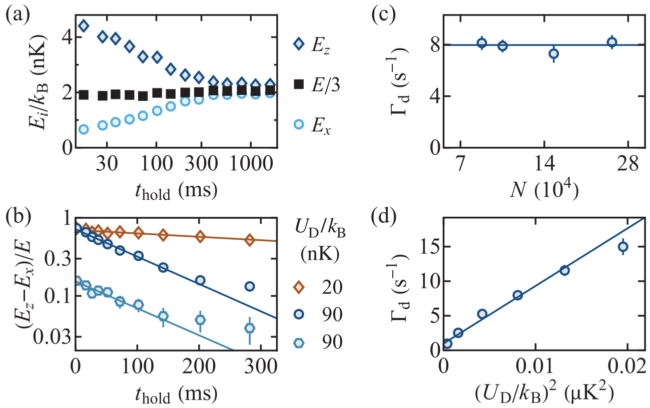

FIG. 3. Disorder-induced cross-dimensional coupling. (a) Here we stop the drive with $U_s/k_B = 10.5$ nK and $\omega_s/(2\pi) = 10$ Hz after $t_s = 0.1$ s [see Fig. 1(b)] and then hold the gas for a variable time t_{hold} in a trap with $U_D/k_B = 90$ nK. The energies E_z and E_x both relax toward $E/3 = (E_z + 2E_x)/3$ (by symmetry $E_x = E_y$). (b) The decay of the anisotropy $(E_z - E_x)/E$ is initially exponential, $\propto \exp(-\Gamma_d t_{hold})$ (solid lines); Γ_d grows with disorder strength ($\propto U_D$) and is independent of the initial anisotropy. (c) As expected for single-particle scattering, Γ_d is independent of the gas density ($\propto N$); here $U_D/k_B = 90$ nK. (d) Dependence of Γ_d on U_D. Up to a small offset of 1 s^{-1}, the data are captured by our numerical simulations with rms disorder equal to 2% of U_D (solid line).

stop the drive, and study the subsequent cross-dimensional relaxation for different disorder strengths ($\propto U_D$). In Fig. 3(a) we show an example of how E_z and E_x both approach $E/3$, and in Fig. 3(b) we show how the anisotropy $(E_z - E_x)/E$ decays for different U_D. The initial decay is captured well by an exponential (solid lines), and we use the decay constant Γ_d as a measure of the typical scattering rate [62]. At long times, the anisotropy decay slows down, which we also observe in simulations of the Schrödinger equation with disorder [42], and attribute to the quantization of states in a finite-size box [63]. In Fig. 3(c) we show that, as expected for single-particle scattering, Γ_d is independent of the particle density.

In Fig. 3(d) we show the dependence of Γ_d on U_D. The solid line is based on our numerical simulations [42], which give $\Gamma_d \propto U_D^2$, as expected from perturbation theory. We match the data well by setting the rms disorder strength to 2% of U_D, and adding a small offset to Γ_d. The 2% disorder is compatible with $\approx$1% observed in the bench tests of the optical potentials used for our box trap [60] (see also [59,64]), and also with the measurements with atoms in Ref. [61], where the uniformity of the gas density was confirmed down to energies of a few % of U_D. In simulations we assume that the disorder is uncorrelated down to a length scale of 800 nm, set by the simulation grid, which is comparable with the expected correlation length of experimental disorder, set by the trap-laser wavelength, $\lambda = 532$ nm. The small offset in Γ_d could arise from trap-shape imperfections or magnetic-field inhomogeneity.

We now turn to the study of the long-time isotropic dynamics for continuous driving (Fig. 4). Here, we take images along the drive axis $\mathbf{z}$, which avoids the small effects of the center-of-mass oscillation [42]. The distribution in the k_x-k_y plane is always isotropic, $n_k(k_x, k_y) = n_k(k_r)$, where $k_r = (k_x^2 + k_y^2)^{1/2}$. We normalize $\int 2\pi k_r n_k(k_r) dk_r = 1$ and define $E_r = E_x + E_y$, so $E_r \approx 2E/3$ for long t_s.

In Fig. 4(a) we plot $N(t_s)$ and $E_r(t_s)$ for $U_s/k_B = 7.0$ nK, $\omega_s/(2\pi) = 10$ Hz, and $\Gamma_d = 8.0$ s^{-1}. At $t_s \approx 15$ s some atoms reach the momentum-space trap depth $k_D = \sqrt{2mU_D/\hbar^2} = 3.8$ μm^{-1}, at which point N starts dropping and E_r saturates. Until then, N is essentially constant [65] and E_r shows power-law growth, $E_r \propto t_s^\eta$, with $\eta = 0.46(2)$.

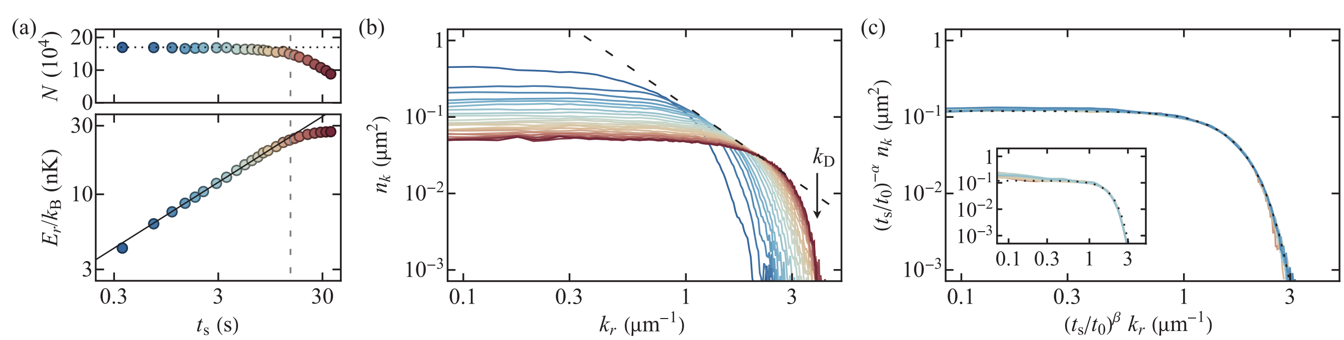

FIG. 4. Subdiffusive dynamic scaling; here, $U_s/k_B = 7.0$ nK, $\omega_s/(2\pi) = 10$ Hz, and $\Gamma_d = 8.0$ s^{-1}. (a) Evolution of the atom number N and the radial per-particle energy E_r. For $t_s \lesssim 15$ s (vertical dashed line), N is essentially constant [65], while $E_r \propto t_s^\eta$ with $\eta = 0.46$ (solid line); at longer t_s some particles have enough energy to leave the trap, so N drops and E_r saturates. (b) Evolution of the radial momentum distribution $n_k(k_r)$; each curve corresponds to a point in (a), with the same color coding. The dashed line, $\propto k_r^{-2}$, is tangent to all the self-similar curves, and k_D is the momentum-space trap depth. (c) For scaling exponents $\alpha = -0.45$ and $\beta = -0.23$ (and arbitrarily chosen reference time $t_0 = 3$ s), the distributions for $t_s \in [1.1, 14.4]$ s and all k_r collapse onto a universal curve. The dotted line shows a compressed-exponential fit, $f_{ce} \propto \exp[-(k_r/k_0)^\kappa]$, with $\kappa = 3.0$ (see text). The inset shows the results of numerical simulations with the same drive, disorder, and scaling parameters (see text and [42]); for comparison with the experiments, the dotted line is the same as in the main panel.

In Fig. 4(b) we show the evolution of $n_k(k_r)$. For $t_s \gtrsim 1$ s the distributions are self-similar, with a well-defined front moving towards the UV until it reaches k_D; for $t_s \gtrsim 15$ s the distribution is essentially stationary.

The fact that n_k is self-similar for $1\text{s} \lesssim t_s \lesssim 15$ s, while E_r grows algebraically, implies dynamic scaling:

$$n_k(k_r, t_s) = \left(\frac{t_s}{t_0}\right)^{\alpha} n_k\left(\left(\frac{t_s}{t_0}\right)^{\beta} k_r, t_0\right), \qquad (2)$$

with $\beta = -\eta/2$, reflecting the subdiffusive energy growth, and $\alpha = 2\beta$, reflecting a particle-conserving transport; t_0 is an arbitrary reference time.

In Fig. 4(c) we show that, for $t_s \in [1.1, 14.4]$ s and all k_r, the distributions can be collapsed onto a universal curve, with $\alpha = -0.45(2)$ and $\beta = -0.23(1)$ [42]. The calculations in [45] predict such scaling with the 3D momentum distribution captured by a compressed exponential, $\propto \exp[-(k/k_0')^{\kappa_{3D}}]$, with κ_{3D} varying between 4 (for $\eta = 1/2$) and 5 (for $\eta = 2/5$), and $k_0' \propto t_s^{1/\kappa_{3D}}$ [66]. We empirically find that $n_k(k_r)$, obtained by integrating the 3D distribution along k_z, is captured by a normalized compressed exponential $f_{ce} = [\pi k_0^2 \Gamma(1 + 2/\kappa)]^{-1} \exp[-(k_r/k_0)^{\kappa}]$ with a reduced $\kappa = 3.0(2)$ [dotted line in Fig. 4(c)] [67]. As shown in the inset of Fig. 4(c), we reproduce our observations in numerical simulations; here we show the results of simulations for $t_s \in [2.9, 18]$ s, obtained with the same U_s, ω_s, and Γ_d, and collapsed with the same α, β, and t_0 as in the experiments.

Repeating our experiments with various drive and disorder parameters, for $U_s/k_B \in$ [3.5, 10.5] nK, $\omega_s/(2\pi) \in$ [5, 15] Hz, and $\Gamma_d \in$ [2.5, 15] s^{-1}, we robustly observe dynamic scaling with $\eta = 0.46(2)$, $\alpha = -0.47(4)$, $\beta = -0.24(2)$, and $\kappa = 2.9(2)$. For our parameters, η is indeed expected to be in the broad crossover from 1/2 to 2/5 [45].

We conclude by pointing to an interesting question for future study: what happens if the drive, the disorder, and the interactions all play a significant role? In the noninteracting ($a = 0$) dynamics observed here, the rate at which energy is absorbed from the drive decays as $t_s^{\eta-1}$. On the other hand, in interacting wave-turbulent cascades [17,49–51] this rate is constant and the turbulent steady state is characterized by $n_k(k_r) \propto k_r^{-\gamma+1}$, with $\gamma = 3.3(3)$. The two types of dynamics are qualitatively different, but are continuously connected by tuning a, as we illustrate in Fig. 5(a) for one set of drive and disorder parameters, and fixed gas density ($\propto N$). This crossover should be controlled by some dimensionless parameter(s), but from the drive, disorder, and interaction properties, one can construct many candidates. Moreover, further qualitatively different outcomes are possible: for strong-enough interactions, thermalization should be the fastest process, while for strong-enough disorder, localization effects should prevail. Constructing the full dynamical phase diagram for the driven and disordered interacting gas is thus a fascinating challenge. As a first step in this direction, in Fig. 5(b) we show that for our parameters the crossover from an energy-space random walk to turbulence depends on the product Na, which suggests that it can be captured within the mean-field Gross–Pitaevskii framework.

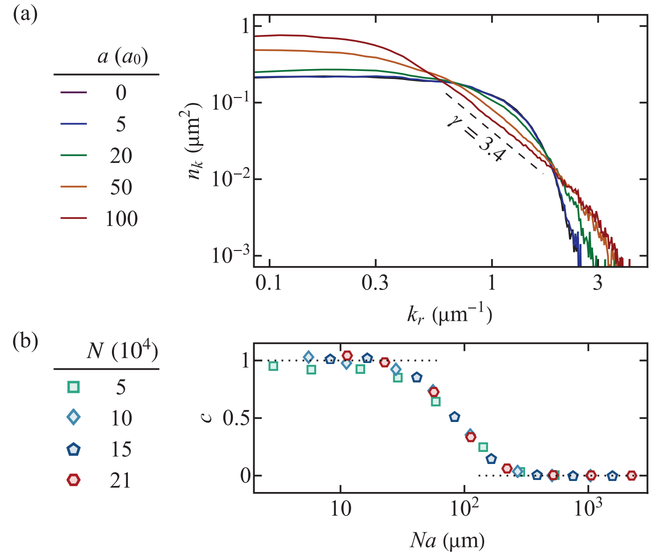

FIG. 5. Crossover from subdiffusion to turbulence, for $U_s/k_B = 7.0$ nK, $\omega_s/(2\pi) = 10$ Hz, $\Gamma_d = 15$ s^{-1}, and $t_s = 1$ s. (a) n_k for $N = 10^5$ atoms and different scattering lengths a. For subdiffusion, n_k is captured by a compressed exponential f_{ce}. For a turbulent cascade, $n_k \propto k_r^{-\gamma+1}$ (dashed line) for $k_r \gtrsim 1/\xi$, where ξ is the healing length; here, $1/\xi = 0.6$ μm^{-1} for 100 a_0. (b) We quantify the crossover between the two regimes by fitting $n_k = c f_{ce}(k_r) + n_0 k_r^{-\gamma+1}$ (with $\gamma = 3.4$) for 0.6 μm$^{-1} < k_r < 2.5$ μm^{-1}, with c and n_0 as free parameters. For various N and a, the crossover from $c = 1$ (subdiffusion) to $c = 0$ (turbulence) depends only on the product Na.

In summary, we have observed subdiffusive dynamic scaling in a noninteracting Bose gas driven far from equilibrium in the presence of weak disorder, which we explain in terms of an energy-space random walk. The tunability of our system opens the possibility to study the interplay of the drive, disorder, and interactions in regimes where they all play a significant role, which we illustrate by showing how the energy-space random walk crosses over to turbulent-cascade dynamics. Our far-from-equilibrium states with low and tuneable energy per particle also provide a novel starting point for studies of equilibration in closed quantum systems [24,25,68].

The data that support the findings of this study are available in the Apollo repository [69].

We thank Nigel R. Cooper, Nir Navon, Maxim Olshanii, and Theo Geisel for discussions, and Robert P. Smith, Jake A. P. Glidden, Lena H. Dogra, Timon A. Hilker, and Samuel J. Garratt for early contributions. This work was supported by EPSRC [Grants No. EP/N011759/1 and No. EP/P009565/1], ERC (UniFlat), and STFC [Grant No. ST/T006056/1]. A. C. acknowledges support from the NSF Graduate Research Fellowship Program (Grant No. DGE2040434). Z. H. acknowledges support from the Royal Society Wolfson Fellowship. C. E. acknowledges support from Jesus College (Cambridge).

*Present address: JILA, NIST, and Department of Physics, University of Colorado, Boulder, Colorado 80309, USA.
†Corresponding author: ce330@cam.ac.uk

[1] S. Fishman, D. R. Grempel, and R. E. Prange, Chaos, quantum recurrences, and Anderson localization, Phys. Rev. Lett. **49**, 509 (1982).

[2] O. Bohigas, M. J. Giannoni, and C. Schmit, Characterization of chaotic quantum spectra and universality of level fluctuation laws, Phys. Rev. Lett. **52**, 1 (1984).

[3] A. J. Lichtenberg and M. A. Lieberman, *Regular and Chaotic Dynamics* (Springer, New York, New York, 1992).

[4] H.-J. Stöckmann, *Quantum Chaos: An Introduction* (Cambridge University Press, Cambridge, 1999).

[5] A. N. Kolmogorov, The local structure of turbulence in incompressible viscous fluid for very large Reynolds numbers, Dokl. Akad. Nauk SSSR **30**, 299 (1941).

[6] A. Obukhov, On the distribution of energy in the spectrum of turbulent flow, Dokl. Akad. Nauk SSSR **32**, 22 (1941).

[7] V. E. Zakharov, V. S. L'vov, and G. Falkovich, *Kolmogorov Spectra of Turbulence* (Springer, Berlin, Heidelberg, 1992).

[8] F. Family and T. Vicsek, Scaling of the active zone in the Eden process on percolation networks and the ballistic deposition model, J. Phys. A **18**, L75 (1985).

[9] M. Kardar, G. Parisi, and Y.-C. Zhang, Dynamic scaling of growing interfaces, Phys. Rev. Lett. **56**, 889 (1986).

[10] M. F. Shlesinger, G. M. Zaslavsky, and J. Klafter, Strange kinetics, Nature (London) **363**, 31 (1993).

[11] R. Metzler and J. Klafter, The random walk's guide to anomalous diffusion: A fractional dynamics approach, Phys. Rep. **339**, 1 (2000).

[12] Y. Sagi, M. Brook, I. Almog, and N. Davidson, Observation of anomalous diffusion and fractional self-similarity in one dimension, Phys. Rev. Lett. **108**, 093002 (2012).

[13] M. Prüfer, P. Kunkel, H. Strobel, S. Lannig, D. Linnemann, C.-M. Schmied, J. Berges, T. Gasenzer, and M. K. Oberthaler, Observation of universal dynamics in a spinor Bose gas far from equilibrium, Nature (London) **563**, 217 (2018).

[14] S. Erne, R. Bücker, T. Gasenzer, J. Berges, and J. Schmiedmayer, Universal dynamics in an isolated one-dimensional Bose gas far from equilibrium, Nature (London) **563**, 225 (2018).

[15] R. Bouganne, M. Bosch Aguilera, A. Ghermaoui, J. Beugnon, and F. Gerbier, Anomalous decay of coherence in a dissipative many-body system, Nat. Phys. **16**, 21 (2020).

[16] J. A. P. Glidden, C. Eigen, L. H. Dogra, T. A. Hilker, R. P. Smith, and Z. Hadzibabic, Bidirectional dynamic scaling in an isolated Bose gas far from equilibrium, Nat. Phys. **17**, 457 (2021).

[17] M. Gałka, P. Christodoulou, M. Gazo, A. Karailiev, N. Dogra, J. Schmitt, and Z. Hadzibabic, Emergence of isotropy and dynamic scaling in 2D wave turbulence in a homogeneous Bose gas, Phys. Rev. Lett. **129**, 190402 (2022).

[18] D. Wei, A. Rubio-Abadal, B. Ye, F. Machado, J. Kemp, K. Srakaew, S. Hollerith, J. Rui, S. Gopalakrishnan, N. Y. Yao, I. Bloch, and J. Zeiher, Quantum gas microscopy of Kardar–Parisi–Zhang superdiffusion, Science **376**, 716 (2022).

[19] M. K. Joshi, F. Kranzl, A. Schuckert, I. Lovas, C. Maier, R. Blatt, M. Knap, and C. F. Roos, Observing emergent hydrodynamics in a long-range quantum magnet, Science **376**, 720 (2022).

[20] Q. Fontaine, D. Squizzato, F. Baboux, I. Amelio, A. Lemaître, M. Morassi, I. Sagnes, L. Le Gratiet, A. Harouri, M. Wouters, I. Carusotto, A. Amo, M. Richard, A. Minguzzi, L. Canet, S. Ravets, and J. Bloch, Kardar–Parisi–Zhang universality in a one-dimensional polariton condensate, Nature (London) **608**, 687 (2022).

[21] A. D. García-Orozco, L. Madeira, M. A. Moreno-Armijos, A. R. Fritsch, P. E. S. Tavares, P. C. M. Castilho, A. Cidrim, G. Roati, and V. S. Bagnato, Universal dynamics of a turbulent superfluid Bose gas, Phys. Rev. A **106**, 023314 (2022).

[22] S. Huh, K. Mukherjee, K. Kwon, J. Seo, S. I. Mistakidis, H. R. Sadeghpour, and J.-Y. Choi, Universality class of a spinor Bose-Einstein condensate far from equilibrium, Nat. Phys. (2024).

[23] S. Lannig, M. Prüfer, Y. Deller, I. Siovitz, J. Dreher, T. Gasenzer, H. Strobel, and M. K. Oberthaler, Observation of two non-thermal fixed points for the same microscopic symmetry, arXiv:2306.16497.

[24] M. Gazo, A. Karailiev, T. Satoor, C. Eigen, M. Gałka, and Z. Hadzibabic, Universal coarsening in a homogeneous two-dimensional Bose gas, arXiv:2312.09248.

[25] J. Berges, A. Rothkopf, and J. Schmidt, Nonthermal fixed points: Effective weak coupling for strongly correlated systems far from equilibrium, Phys. Rev. Lett. **101**, 041603 (2008).

[26] P. W. Anderson, Absence of diffusion in certain random lattices, Phys. Rev. **109**, 1492 (1958).

[27] K. von Klitzing, The quantized Hall effect, Rev. Mod. Phys. **58**, 519 (1986).

[28] B. L. Altshuler, D. Khmel'nitzkii, A. I. Larkin, and P. A. Lee, Magnetoresistance and Hall effect in a disordered two-dimensional electron gas, Phys. Rev. B **22**, 5142 (1980).

[29] F. Evers and A. D. Mirlin, Anderson transitions, Rev. Mod. Phys. **80**, 1355 (2008).

[30] A. H. Castro Neto, F. Guinea, N. M. R. Peres, K. S. Novoselov, and A. K. Geim, The electronic properties of graphene, Rev. Mod. Phys. **81**, 109 (2009).

[31] *Scattering and Localization of Classical Waves in Random Media*, edited by P. Sheng (World Scientific, Singapore, 1990).

[32] G. Labeyrie, F. de Tomasi, J.-C. Bernard, C. A. Müller, C. Miniatura, and R. Kaiser, Coherent backscattering of light by cold atoms, Phys. Rev. Lett. **83**, 5266 (1999).

[33] J. Billy, V. Josse, Z. Zuo, A. Bernard, B. Hambrecht, P. Lugan, D. Clément, L. Sanchez-Palencia, P. Bouyer, and A. Aspect, Direct observation of Anderson localization of matter waves in a controlled disorder, Nature (London) **453**, 891 (2008).

[34] G. Roati, C. D'Errico, L. Fallani, M. Fattori, C. Fort, M. Zaccanti, G. Modugno, M. Modugno, and M. Inguscio, Anderson localization of a non-interacting Bose–Einstein condensate, Nature (London) **453**, 895 (2008).

[35] R. Nandkishore and D. A. Huse, Many-body localization and thermalization in quantum statistical mechanics, Annu. Rev. Condens. Matter Phys. **6**, 15 (2015).

[36] M. Schreiber, S. S. Hodgman, P. Bordia, H. P. Lüschen, M. H. Fischer, R. Vosk, E. Altman, U. Schneider, and I. Bloch, Observation of many-body localization of interacting fermions in a quasirandom optical lattice, Science **349**, 842 (2015).

[37] D. A. Abanin, E. Altman, I. Bloch, and M. Serbyn, Colloquium: Many-body localization, thermalization, and entanglement, Rev. Mod. Phys. **91**, 021001 (2019).

[38] J. Zhang, P. W. Hess, A. Kyprianidis, P. Becker, A. Lee, J. Smith, G. Pagano, I.-D. Potirniche, A. C. Potter, A. Vishwanath, N. Y. Yao, and C. Monroe, Observation of a discrete time crystal, Nature (London) **543**, 217 (2017).

[39] S. Choi, J. Choi, R. Landig, G. Kucsko, H. Zhou, J. Isoya, F. Jelezko, S. Onoda, H. Sumiya, V. Khemani, C. von Keyserlingk, N. Y. Yao, E. Demler, and M. D. Lukin, Observation of discrete time-crystalline order in a disordered dipolar many-body system, Nature (London) **543**, 221 (2017).

[40] D. V. Else, C. Monroe, C. Nayak, and N. Y. Yao, Discrete time crystals, Annu. Rev. Condens. Matter Phys. **11**, 467 (2020).

[41] P. Kongkhambut, J. Skulte, L. Mathey, J. Cosme, A. Hemmerich, and H. Keßler, Observation of a continuous time crystal, Science **377**, 670 (2022).

[42] See Supplemental Material at http://link.aps.org/supplemental/10.1103/PhysRevLett.132.113401 for details on our numerical simulations (Sec. I), the frequency response of our noninteracting gas (Sec. II), the extraction of the dynamic-scaling exponents (Sec. III), and the robustness of the dynamic-scaling behavior (Sec. IV).

[43] L. E. Reichl and W. A. Lin, Exact quantum model of field-induced resonance overlap, Phys. Rev. A **33**, 3598 (1986).

[44] W. A. Lin and L. E. Reichl, Spectral analysis of quantum-resonance zones, quantum Kolmogorov-Arnold-Moser theorem, and quantum-resonance overlap, Phys. Rev. A **37**, 3972 (1988).

[45] Y. Zhang, G. Martirosyan, C. J. Ho, J. Etrych, C. Eigen, and Z. Hadzibabic, Energy-space random walk in a driven disordered Bose gas, C. R. Phys. (2023).

[46] C. Jarzynski, Energy diffusion in a chaotic adiabatic billiard gas, Phys. Rev. E **48**, 4340 (1993).

[47] G. Bunin, L. D'Alessio, Y. Kafri, and A. Polkovnikov, Universal energy fluctuations in thermally isolated driven systems, Nat. Phys. **7**, 913 (2011).

[48] W. Hodson and C. Jarzynski, Energy diffusion and absorption in chaotic systems with rapid periodic driving, Phys. Rev. Res. **3**, 013219 (2021).

[49] N. Navon, A. L. Gaunt, R. P. Smith, and Z. Hadzibabic, Emergence of a turbulent cascade in a quantum gas, Nature (London) **539**, 72 (2016).

[50] N. Navon, C. Eigen, J. Zhang, R. Lopes, A. L. Gaunt, K. Fujimoto, M. Tsubota, R. P. Smith, and Z. Hadzibabic, Synthetic dissipation and cascade fluxes in a turbulent quantum gas, Science **366**, 382 (2019).

[51] L. H. Dogra, G. Martirosyan, T. A. Hilker, J. A. P. Glidden, J. Etrych, A. Cao, C. Eigen, R. P. Smith, and Z. Hadzibabic, Universal equation of state for wave turbulence in a quantum gas, Nature (London) **620**, 521 (2023).

[52] We convolve the equilibrium Bose distribution with a Gaussian of width 0.3 μm^{-1} (our k-space resolution [53]).

[53] Our k-space resolution, given by the box size and the 50-ms time-of-flight duration, is ≈0.3 μm^{-1}.

[54] A. L. Gaunt, T. F. Schmidutz, I. Gotlibovych, R. P. Smith, and Z. Hadzibabic, Bose–Einstein condensation of atoms in a uniform potential, Phys. Rev. Lett. **110**, 200406 (2013).

[55] C. Eigen, A. L. Gaunt, A. Suleymanzade, N. Navon, Z. Hadzibabic, and R. P. Smith, Observation of weak collapse in a Bose–Einstein condensate, Phys. Rev. X **6**, 041058 (2016).

[56] N. Navon, R. P. Smith, and Z. Hadzibabic, Quantum gases in optical boxes, Nat. Phys. **17**, 1334 (2021).

[57] M. Fattori, G. Roati, B. Deissler, C. D'Errico, M. Zaccanti, M. Jona-Lasinio, L. Santos, M. Inguscio, and G. Modugno, Magnetic dipolar interaction in a Bose–Einstein condensate atomic interferometer, Phys. Rev. Lett. **101**, 190405 (2008).

[58] J. Etrych, G. Martirosyan, A. Cao, J. A. P. Glidden, L. H. Dogra, J. M. Hutson, Z. Hadzibabic, and C. Eigen, Pinpointing Feshbach resonances and testing Efimov universalities in ^{39}K, Phys. Rev. Res. **5**, 013174 (2023).

[59] A. L. Gaunt and Z. Hadzibabic, Robust digital holography for ultracold atom trapping, Sci. Rep. **2**, 721 (2012).

[60] A. L. Gaunt, Degenerate Bose gases: Tuning interactions & geometry, Ph.D. thesis, University of Cambridge, 2014.

[61] I. Gotlibovych, T. F. Schmidutz, A. L. Gaunt, N. Navon, R. P. Smith, and Z. Hadzibabic, Observing properties of an interacting homogeneous Bose–Einstein condensate: Heisenberg-limited momentum spread, interaction energy, and free-expansion dynamics, Phys. Rev. A **89**, 061604(R) (2014).

[62] Note that in reality the k-dependent scattering rate is different for different particles.

[63] The semiclassical picture in Fig. 2 assumes a continuum of states. In reality, states are quantized and "elastic" scattering is possible only if there is a final state with energy within $\approx\hbar\Gamma_\mathrm{d}$ of the initial one. In our weak disorder, $\hbar\Gamma_\mathrm{d}$ is never much larger than the energy-quantization scale $\hbar^2\pi^2/(2mL^2) = h \times 0.5$ Hz, so the scattering may not be fully isotropic.

[64] P. Schroff, A. La Rooij, E. Haller, and S. Kuhr, Accurate holographic light potentials using pixel crosstalk modelling, Sci. Rep. **13**, 3252 (2023).

[65] Without a drive, N decays very slowly, with a 1-body lifetime of 140 s, due to collisions with the background vapor in the vacuum chamber. On average, these losses do not change E.

[66] Also note that for the dynamic scaling of the 3D distribution $\alpha = 3\beta$, with the same β as for $n_k(k_r)$.

[67] Integrating a 3D compressed exponential along k_z does not analytically give another compressed exponential, but this is a good approximation in the experimental k range.

[68] I. Chantesana, A. P. Orioli, and T. Gasenzer, Kinetic theory of nonthermal fixed points in a Bose gas, Phys. Rev. A **99**, 043620 (2019).

[69] https://doi.org/10.17863/CAM.105358.